

Study on the Formulation Mechanism of Blisters in Electrochemical Hydriding Experiment of Medium Carbon Steel through Macro-micro Simulation

*Li Yuan, **Du Fengshan, ***Fan Junkai, ****Huang Shiguang, *****Hu Binbin

*School of Mechanical Engineering, Yanshan University
China, Hebei, (cccruler234@hotmail.com)

**School of Mechanical Engineering, Yanshan University
China, Hebei, (fsdu@ysu.edu.cn)

***School of Mechanical and Power Engineering, Henan Polytechnic University
China, Henan, (29656632@qq.com)

****School of Mechanical Engineering, Yanshan University
China, Hebei, (1571776058@qq.com)

*****School of Mechanical Engineering, Yanshan University
China, Hebei, (904241905@qq.com)

Abstract

With medium carbon steel as the research object, this paper explores the regularities of hydrogen diffusion by electrochemical hydriding, establishes a macro-micro hydrogen diffusion simulation model, and obtains the regularities of hydrogen concentration distribution at different initial hydrogen concentrations and different hydriding times. Based on the test results, the authors get reasonable values of parameters that are difficult to measure, such as the initial concentration coefficient α . To disclose the formation mechanism of hydrogen-induced blisters, this paper analyzes the regularities of hydrogen concentration, diffusion and condensation in hydrogen traps from the micro perspective. The macro-micro hydrogen diffusion simulation model offers a simulation method to similar electrochemical experiments, helps predict hydrogen

diffusion and condensation in cases that are difficult to measure, and provides clues to prevent “hydrogen embrittlement”.

Keywords

Electrochemical hydriding, hydrogen diffusion model, hydrogen-induced blisters, hydrogen pressure

1. Introduction

The chemical element hydrogen is very harmful to metals. In the forging process, “Forging flakes” is known as the “cancer” of the forge piece [1]. To better understand the mechanism of hydrogen embrittlement, the electrochemical hydriding method is increasingly applied. The electrochemical hydriding experiment amplifies the hydrogen diffusion and condensation, which are difficult to observe in actual production, so that researchers can make clear observations and disclose the regularities of hydrogen induced damage. In recent years, researchers have taken the method of electrochemical hydriding experiment to study some pipeline steel materials [2-5] and high carbon steel materials [6]. In this paper, an electrochemical hydriding experiment is carried out on medium carbon steel. During the experiment, hydrogen-induced blisters emerge on the surface of hydrogenated carbon steel specimens. As a common form of material degradation caused by hydrogen pressure, hydrogen-induced blister is the ultimate state of “hydrogen embrittlement”. The phenomenon is clearly related to the diffusion and condensation of hydrogen in metals. Hence, the study on the formation mechanism of hydrogen-induced blisters has guiding effect on finding the causes of “hydrogen embrittlement”.

To disclose the formation mechanism of hydrogen-induced blisters, this paper establishes a macro-micro finite element hydrogen diffusion model based on Voronoi cell topology information with the finite element software Abaqus [7], and analyzes the hydrogen diffusion in common hydrogen traps. The simulation results are compared with the results of electrochemical hydriding experiment under the same conditions, which proves that the simulation results are valid and can provide a simulation platform for similar hydrogen damage research.

2. The electrochemical hydriding experiment on medium carbon steel

2.1 The principle of the electrochemical hydriding experiment

The electrochemical hydriding uses electrochemical-atomic diffusion method to apply polarization current on the working medium and to ionize the required hydrogen ions. In the hydriding process, the magnitude of the current can be changed to provide the different hydrogen concentrations required for the experiment.

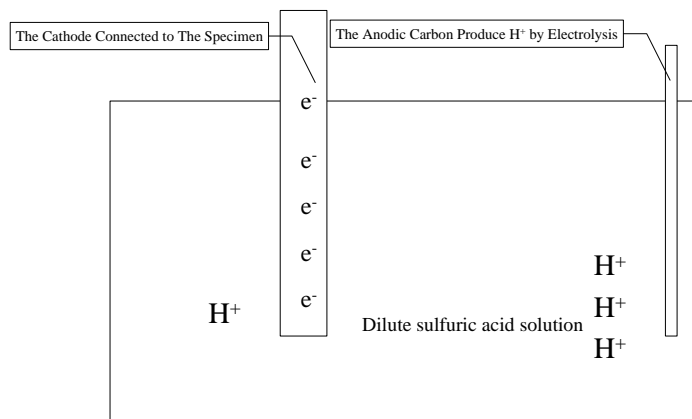


Fig.1. Schematic diagram of electrochemical hydriding experiment



Fig. 2 Equipments of the hydriding experiment

Fig.1 displays the experimental principle of electrochemical hydriding. In the experiment, the hydrogenated specimen, as the working electrode, is connected to the cathode of the power supply and the inert electrode, as the auxiliary electrode, is connected to the anode of the power supply. The electrochemical workstation provides working current for the experiment. When the circuit is connected, the following chemical reactions would take place at the anodic and cathodic terminals of the working electrode:

Anodic terminal:



Cathodic terminal:



Total reaction:



As the electrolyte of the experiment, the dilute sulfuric acid solution contains positive hydrogen ions. The specimen connected to the cathode is negatively charged. Thus, positively charged hydrogen ions are attracted and adsorbed to the surface of the specimen and are diffused into the specimen. The hydrogen ions in the solution are replenished by the anode, which releases hydrogen ions through electrolysis.

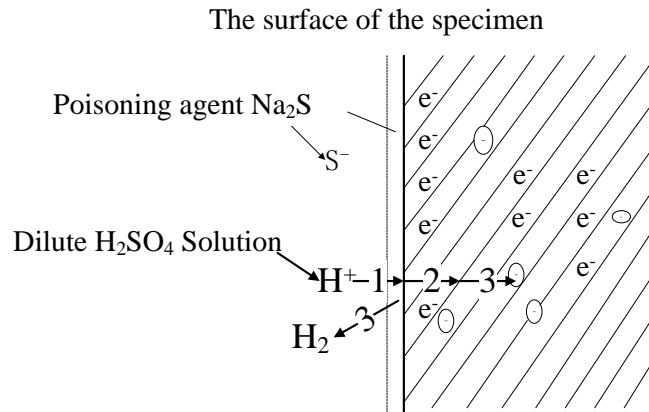


Fig.3. Schematic diagram of hydrogen diffusion in metal

As shown in Fig.2, the permeation of hydrogen into the metal is a complex and continuous process. It can be described by three processes: hydrogen adsorption, diffusion and condensation. Process 1 in Fig.2 refers to hydrogen adsorption, in which the positively charged hydrogen ions in the solution are attracted by the negatively charged specimen and adsorbed to the surface of the specimen. The surface of the specimen is coated with the poisoning agent Na_2S . The inhibition principle of the poisoning agent goes as follows: Since hydrogen sulfide is easily dissolved in water, when S^{2-} is adsorbed to the surface of the electrode, the hydrogen ions are inhibited from forming hydrogen molecules on the electrode surface; thus, hydrogen ions tend to form hydrogen atoms and migrate into the metal specimen. Process 2 refers to hydrogen diffusion. Through Process 1, each of the hydrogen ions gets an electron from within the specimen, thus forming hydrogen atoms. The atoms diffuse from areas of greater concentration to areas of lesser concentration. i.e. down the gradient. Therefore, the hydrogen concentration on the surface of the specimen slowly spreads to the interior. Process 3 refers to hydrogen condensation. The hydrogen atoms produced in Process 2 are not combined into hydrogen molecules in places of perfect crystal lattice. However, when the hydrogen atoms enter the cavities of the materials, they would condense into hydrogen molecules as the concentration increases. During the condensation, the volume would expand 16 times, resulting in a huge hydrogen pressure and a number of micro-

cracks. When the hydrogen pressure is large enough, the micro-cracks would expand to form macroscopic hydrogen-induced blisters. Part of hydrogen condensation takes place outside the specimen. On encountering electrons, the hydrogen ions in the solution develop into hydrogen atoms. When the concentration of hydrogen atoms is large enough, the atoms would condense into hydrogen molecules, which flow over the electrolytic cell.

2.2 The procedures of the electrochemical hydriding experiment on medium carbon steel

40Cr, a typical type of medium carbon steel, is selected for the experiment. The chemical composition of the steel is shown in Table 1. The 2cm thick specimen has been mechanically polished before hydriding. The hydriding solution is 0.5mol/l of H₂SO₄ with 250gm/l Na₂S as the poisoning agent. The hydriding current densities are 2mA/cm², 6mA/cm² and 10mA/cm². The hydriding times are 1h, 3h, and 5h. The CS series electrochemical workstation (Wuhan Corrtest Instruments Corp., Ltd.) is used in the experiment. All tests are performed at room temperature (about 25°C).

Table 1. The chemical composition of 40Cr (mass fraction, %)

| C | Si | Mn | Cr | P | S | Mo |
|------|------|------|-----|--------|-------|-------|
| 0.41 | 0.23 | 0.94 | 0.8 | <0.035 | <0.04 | 0.015 |

2.3 The results of the electro chemical hydriding experiment on medium carbon steel

According to the experimental results, the surface morphology of 40Cr steel under different charging currents and charging times is as follows:



a) 1h, 2mA/cm²



b) 3h, 2mA/cm²



c) 5h, 2mA/cm²

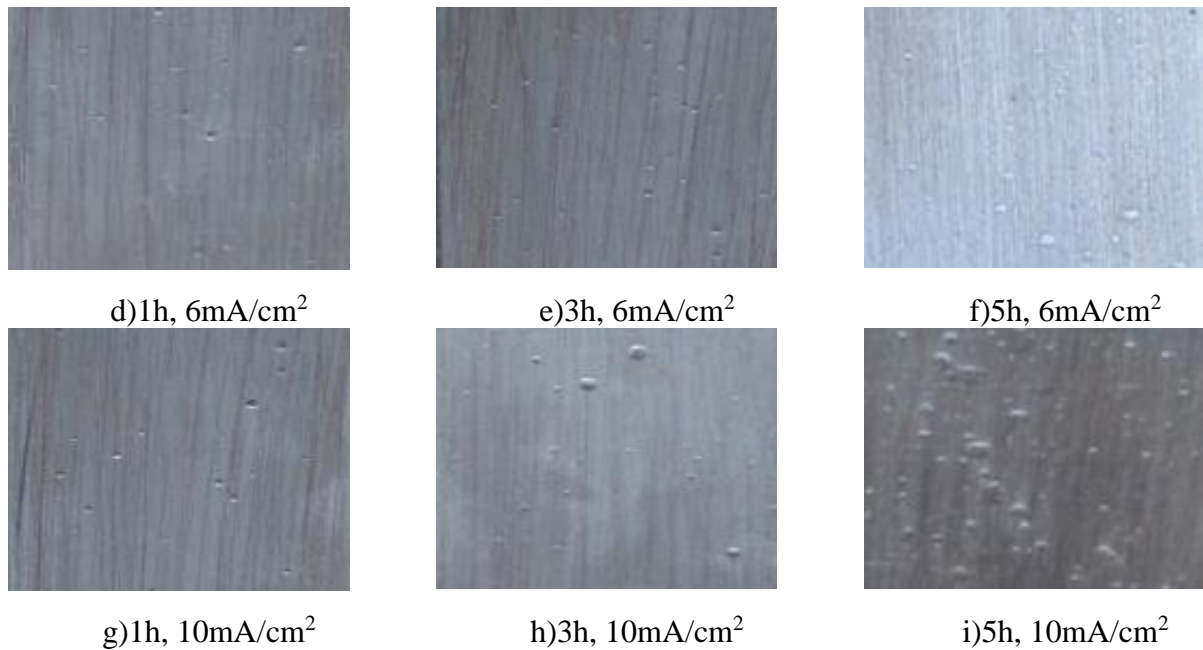


Fig.4. The surface morphology of 40Cr steel under different charging currents and charging times

It can be seen from Fig.4 that the number and significance of blisters on the specimen increases with the hydriding time. At 3h, the hydrogen-induced blisters on the surface of the specimen are dense and small. The blisters are mostly long strips or ovals at the initial stage of hydriding. At 5h, the hydrogen-induced blisters on the surface of the 40Cr specimen grow rapidly in size and density, and become more and more circular in shape. In other words, the hydrogen-induced blisters are significant and clearly visible. When the hydriding current is $10\text{mA}/\text{cm}^2$, the surface of the specimen has visible hydrogen-induced blisters under any of the three hydriding times. As the hydriding current increases, the earlier, the more and the plumper the blisters become. Analysis shows that the hydrogen-induced blisters on the surface of the specimen are mainly formed under the following condition: With more hydrogen atoms diffuse into the specimen, a large number of atoms would accumulate in defective pores of the specimen or dislocation spaces of grains; in this case, the hydrogen atoms are combined into hydrogen molecules, in which the volume expands 16 times^[10]. As the increase in volume results in a huge hydrogen pressure, the formation of blisters is an inevitable way to rebalance the pressure.

2.4 The calculation of electrochemical hydrogen diffusion parameters

In the electrochemical experiment, the hydrogen flow rate through the specimen area is related to the anode current density I_∞ at the steady state. The hydrogen permeation amount J_∞ is expressed as:

$$J_{\infty} = \frac{I_{\infty}}{FA} \quad (6)$$

Where A is the specimen area (cm²) and F is the Faraday constant (96,500C/mol).

The effective hydrogen diffusion coefficient D is calculated as:

$$D_{\text{eff}} = \frac{d^2}{6t_L} \quad (7)$$

Where d is the specimen thickness (cm), t_L is the lag time [1] (s), i.e. the time it takes for the anode current I_t to reach 0.63 I_∞ in the hydrogen permeation curve.

The hydrogen concentration C₀ on the surface of the specimen is calculated as:

$$C_0 = \frac{J_{\infty} \times d}{D_{\text{eff}}} \quad (8)$$

When the hydriding current density is 2mA/cm², C₀ is 2.22x10⁻⁴ mol/cm³, i.e. 57.3ppm; when the hydriding current density is 6mA/cm², C₀ is 6.661x10⁻⁴ mol/cm³, i.e. 171.86ppm; when the hydriding current density is 10mA/cm², C₀ is 1.11x10⁻³mol/cm³, i.e. 286.43ppm.

As shown in Fig.3, in electrolysis hydriding, a large part of the hydrogen atoms condense into hydrogen molecules in Process 3, and flow over the electrolytic cell. Thus, the initial hydrogen concentration of effective hydrogen diffusion should be multiplied by an initial hydrogen concentration correction coefficient α.

The solubility of hydrogen in iron is calculated by the following equations:

$$\begin{aligned} c_H &= 3.7\sqrt{P_{H_2}} \exp\left(-\frac{6500}{RT}\right) \\ &= 4300 \exp\left(-\frac{3261}{T}\right) \\ &= 0.07603\text{ppm mm/N}^{1/2} \end{aligned}$$

Taking α = 0.1, the normalized concentration C_N is 75.36N^{1/2}/mm at the hydriding current density of 2mA/cm², 226.08N^{1/2}/mm at 6mA/cm², and 376.8N^{1/2}/mm at 10mA/cm²; the diffusion coefficient is 1.5459x10⁻⁷cm²/s, and the solubility is 0.07603 ppm mm/N^{1/2}.

3. Macro-micro finite element simulation model for the electrochemical hydriding experiment

A finite element microscopic model based on voronoi cell topology information has been carried on , according to the above experiment, for a further analysis of the concentration of hydrogen diffusion process, and the process of the evolution of hydrogen defects.

3.1 Establishment of the microscopic model based on Voronoi cell topology information

In Voronoi diagram, the position of generators determines the location and size of the Voronoi cells. Therefore, the arrangement of generators is of critical importance to the generation of Voronoi diagram. For a piece of forged metal in the annealed state, its cells can be approximated as uniformly distributed. Thus, the generators of Voronoi diagram should be arranged in uniformity.

Write functions in MATLAB:

$$x=\text{rand}(10n,n)*a+b \tag{5}$$

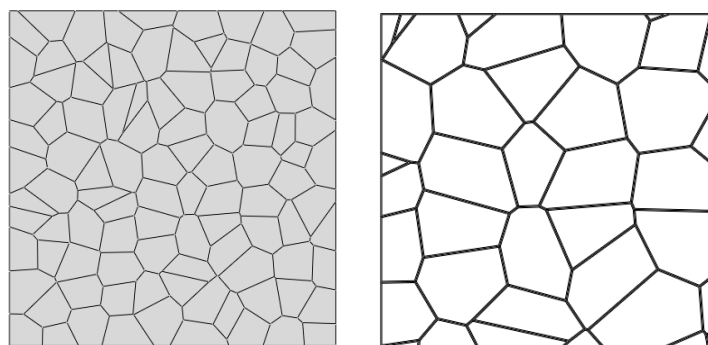
Where, x is the coordinate matrix of the generator of the cell;

a is the critical distance coefficient of the cell;

b is the position range coefficient of the cell;

n is the number of dimensions of the Voronoi diagram.

The Voronoi cell topology information can be obtained by calling the Voronoi function in MATLAB. Then, the topology information of the Voronoi diagram exported from MATLAB is read by using the Script in ABAQUS, and the node coordinates of Voronoi diagram and the node number of each Voronoi cell are transferred to the Part module of ABAQUS. Next, the Part is segmented according to the Voronoi cell topology information. Finally, the grain boundaries are saved.



a) The grain boundaries have not been divided. b) The grain boundaries have been divided.

Fig.5. The microscopic model for Voronoi cells

3.2 The establishment of electrochemical macroscopic hydrogen diffusion model and the microscopic crystal hydrogen diffusion model

According to the principle of the electrochemical experiment, the hydrogen diffusion model can be simplified as a model of hydrogen diffusion along the thickness of the parts. The thermal analysis module DC2D4 is used to divide the grid. The boundary conditions of the left and right sides of the model are set as the curve of the hydrogen concentration C_0 which changes with the hydriding time under the three different current densities. The initial concentration of the remaining nodes is set at 0. A 0.01s long steady state analysis is performed first, followed by the transient analysis. The time is calculated as 18000s. The diffusion coefficient is set at $1.5459 \times 10^{-7} \text{cm}^2/\text{s}$, and the solubility is $0.07603 \text{ ppm mm}/\text{N}^{1/2}$.

After measurement, it is found that hydrogen-induced blisters mostly appear at 0.3 mm to 0.4 mm from the surface. Thus, a representative volume element (RVE) is selected at 0.35 mm from the surface to simulate various hydrogen traps.

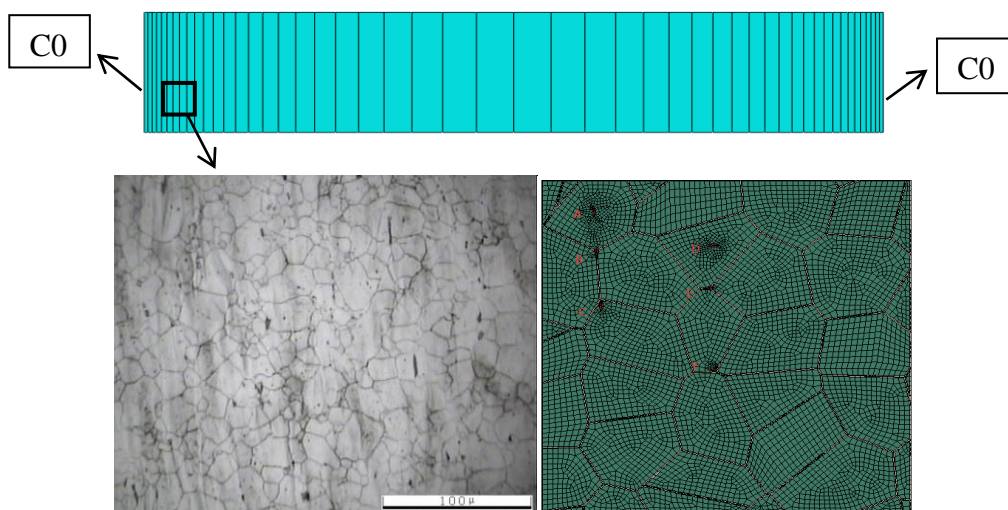


Fig.6. Schematic diagram of the RVE

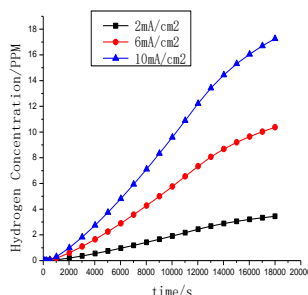


Fig.7. C_0 hydrogen concentration curve

(i.e. the hydrogen concentration boundary conditions of the microscopic model)

3.3 Simulation results of the electrochemical macroscopic hydrogen diffusion model and analysis of the results

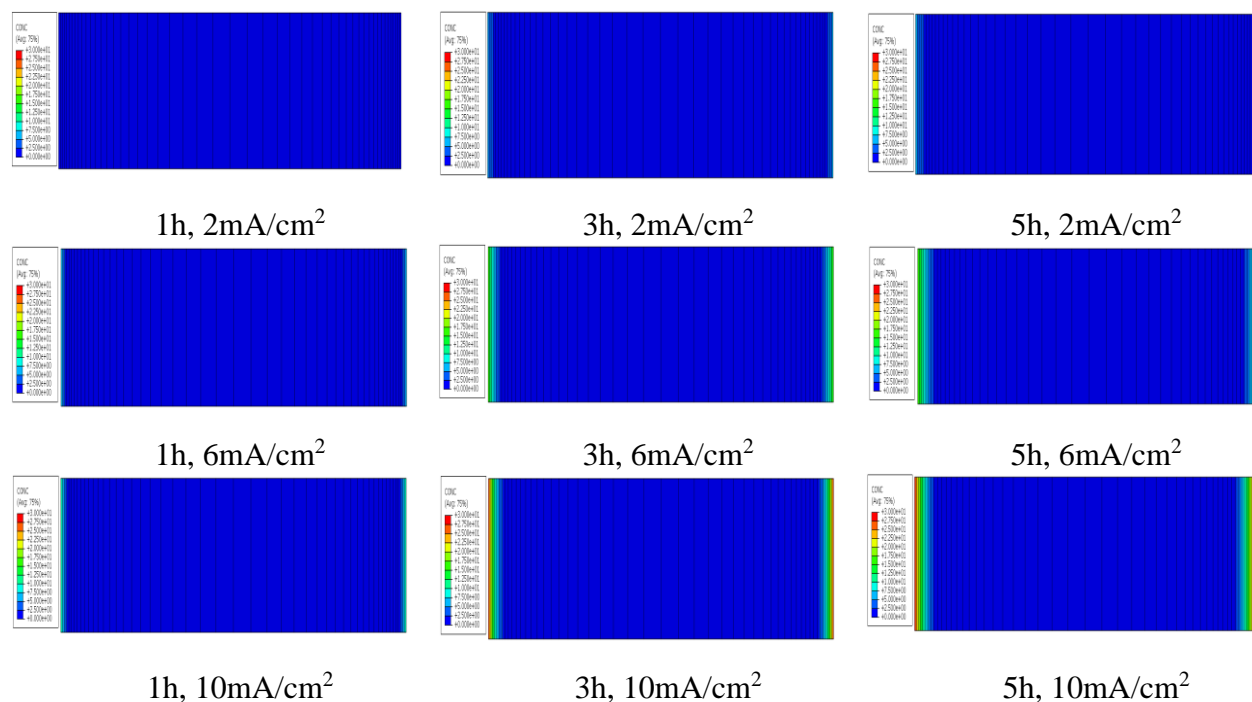


Fig.8. Macroscopic hydrogen diffusion diagram

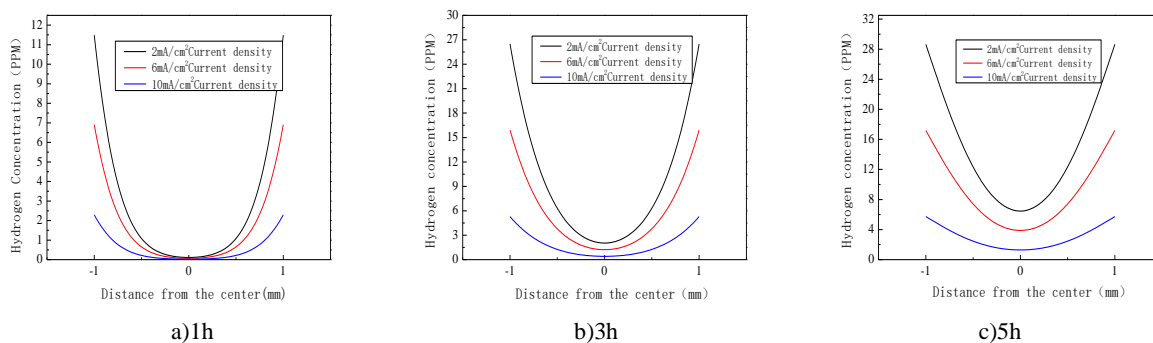


Fig.9. Hydrogen diffusion simulation results with different hydrogen concentration boundary conditions and hydriding time

The simulation results shown in Fig 8-9 demonstrate that: as the hydriding time increases, boundary hydrogen density does not change greatly, but the hydrogen permeability increases. At 5h, the hydrogen concentration at the center of the specimen is close to 6ppm, much higher than 1ppm at 1h. At 1h, the center of the specimen is barely infiltrated, regardless of the external hydrogen concentration boundary condition. The hydrogen concentration at the center of the specimen is not significantly different under the three hydrogen concentration boundary

conditions. Based on the simulation results, the hydrogen concentration remains low at the boundaries and the center of the specimen under the current of $2\text{mA}/\text{cm}^2$ at 5h. This explains why there is almost no blister under $2\text{mA}/\text{cm}^2$ in the experiment, and why the few blisters are long strips or ovals. The hydrogen concentration at the blisters is much higher under $6\text{mA}/\text{cm}^2$ than that under $2\text{mA}/\text{cm}^2$. That is because the hydrogen atoms have more chance to collide with each other as the hydriding time increases; when the atoms combine into hydrogen molecules, the volume expands drastically and results in blisters. Fig 4-e and Fig 4-f are in agreement with the simulation results. The boundary hydrogen concentration is nearly 9ppm under $10\text{mA}/\text{cm}^2$, higher than that under other magnitudes of current. It is clearly displayed in Fig 4-i that, when the hydrogen concentration increases dramatically, the hydrogen-induced blisters grow rapidly in size and density, and become more and more circular in shape. In other words, the hydrogen-induced blisters are significant and clearly visible.

In general, local irregularities, such as cavities, dislocations, grain boundaries and inclusions, are the main hydrogen traps in steel, and hydrogen traps are important for hydrogen-induced blisters and hydrogen-induced cracking influences. The arrangements of the various hydrogen traps are shown in Fig.10

4. Hydrogen trap simulation analysis with microscopic crystal model

Normally, the main hydrogen traps in steel are local irregularities like cavities, dislocations, grain boundaries and inclusions [8,9]. The hydrogen traps have significant influence on hydrogen-induced blisters and cracks. Fig.10 shows various kinds of hydrogen traps.

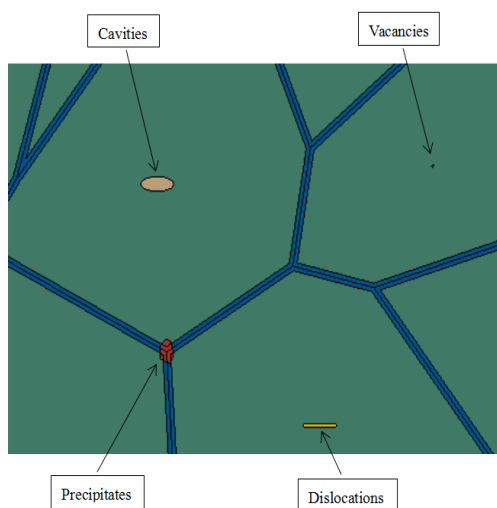


Fig.10. Schematic map of hydrogen traps

At near room temperature, the diffusion coefficient of hydrogen in the grain boundary will be greater than the diffusion coefficient in the lattice. Therefore, in the mesoscopic model, the

hydrogen diffusion coefficient of the grain boundary is set to inherit the diffusion coefficient of the material, and the hydrogen diffusion coefficient of the lattice is several times the hydrogen diffusion coefficient of the material. The hydrogen diffusion coefficient and hydrogen solubility in different hydrogen traps are also different. The hydrogen solubility of the hydrogen trap in the cavities is the largest, followed by the Precipitates, the dislocations, the hydrogen trap at the grain boundary, and lattice vacancies hydrogen trap has the least solubility. In terms of the hydrogen diffusion coefficient, The diffusion coefficient of dislocations hydrogen trap is the largest, followed by the grain boundary of the hydrogen trap, the cavities of the hydrogen trap, the lattice vacancies of the hydrogen trap, and the smallest is Precipitates hydrogen trap.

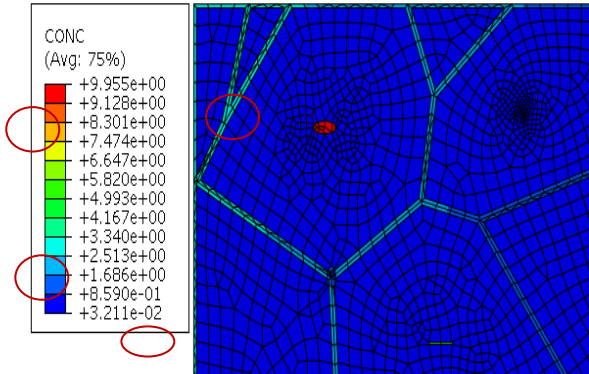


Fig.11. The simulation diagram under 5h, 10mA/cm2

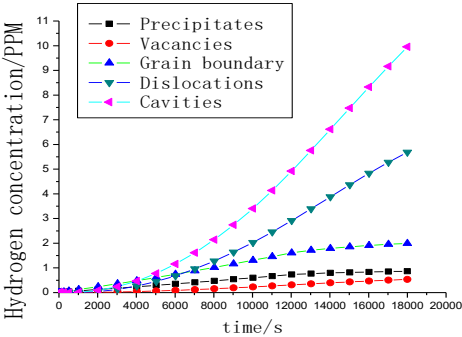


Fig.12. The relation curve between the hydrogen concentrations at various hydrogen traps and the hydriding times

According to the simulation results, the hydrogen concentration is highest at the hydrogen trap of cavities and the lowest at the hydrogen trap of lattice vacancies.

To study the influence of the distribution of hydrogen traps on the hydrogen accumulation, six cavities are arranged in different positions.

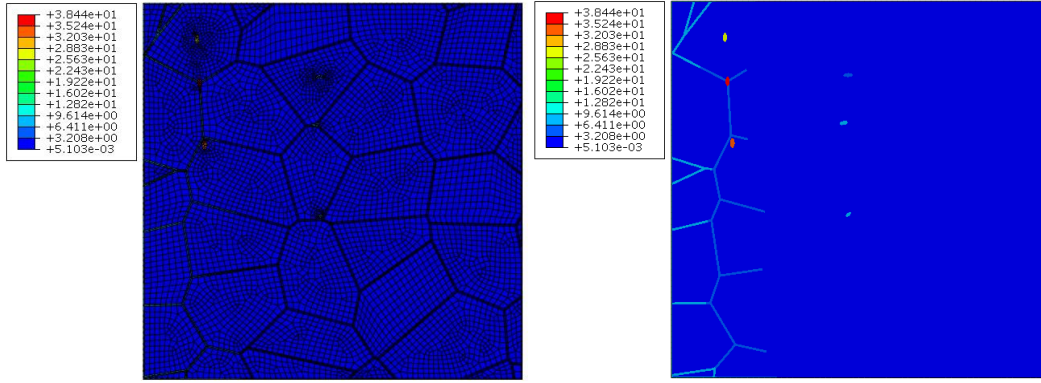


Fig.13. The simulation diagram under 1h, 10mA/cm²

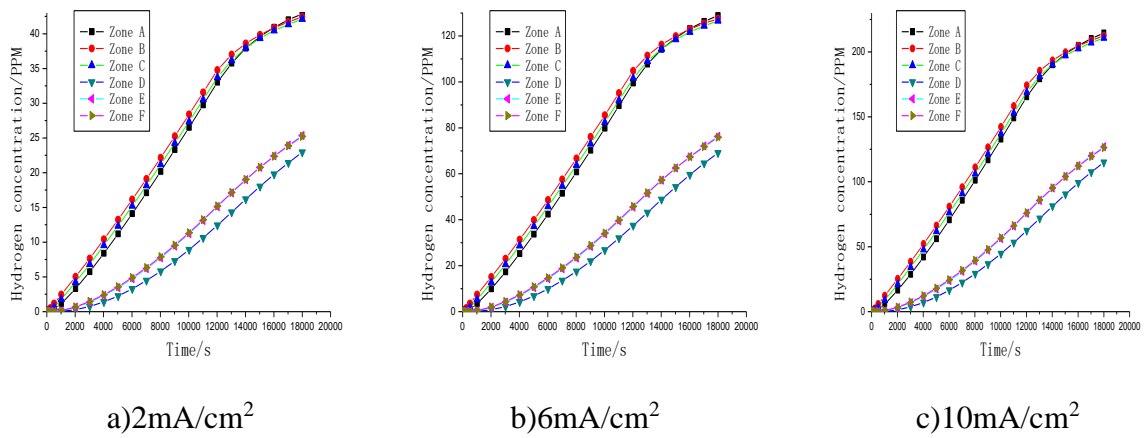


Fig.14. Regional hydrogen concentration under different current magnitudes

According to the simulation results, the hydrogen concentration is significantly higher in A, B and C, which are closer to the diffusion source, than in D, E and F, which are far away from the source, indicating that the concentration at the hydrogen trap is closely related to the depth of the trap. This echoes the experimental results. In the experiment, hydrogen-induced blisters emerge at 0.3-0.5mm from the surface. Leaving out the thickness of the surface oxide layer, the blisters are basically inversely proportional to the depth of the hydrogen trap. Comparing the regions A, B and C with the regions D, E and F, the authors discover that Region B, located right on the grain boundary, has a higher hydrogen concentration at hydrogen trap than the traps of the same depth in the other two regions; close to the grain boundary, Region C has a slightly lower concentration; situated inside the lattice, Region A has the lowest concentration.

5. Conclusion

1) The electrochemical hydriding experiment shows that, with the increase in current density and hydriding time, more and more hydrogen-induced blisters are produced on the surface of medium carbon steel, and the blisters are increasingly plump.

2) The authors obtain the relation between hydrogen concentration and time through the numerical simulation of the hydrogen diffusion in carbon steel by the finite element software ABAQUS. The findings are in good agreement with the morphology of blisters on the surface of carbon steel in the experiment, indicating that the finite element model is reliably. The method offers a simulation platform to similar electrochemical experiments, helps predict hydrogen diffusion and condensation in cases that are difficult to measure, and provides clues to prevent “hydrogen embrittlement”.

3) On the basis of macroscopic hydrogen diffusion model, the authors further explore the formation mechanism of blisters with the microscopic hydrogen trap model. The results signify that the formation of hydrogen-induced blisters is related to the depth of hydrogen trap. The deeper the trap, the lower the hydrogen concentration, and the more difficult it is to form hydrogen-induced blisters. The formation of hydrogen-induced blisters is also relevant to the location of the hydrogen trap relative to the grain boundary. The traps closer to the boundary are easier to form blisters. In addition, the formation has something to do with the state of the trap. Blisters are most likely formed in cavities.

References

1. D.T. Kang, Materials and heat treatment of large forging, Beijing: Longmen Book Company, 1998: 106-108.
2. J. Li, F.S. Du, Y. Liang, S. Wu, T.Y. Tan, Hydrogen diffusion calculation experiment of the sheet metal, 2016, Iron and steel, vol. 51, no. 7, pp.70-75.
3. G. Chen, L.P. Wang, Fracture properties of different pipeline steels at electrochemical hydrogen charging state, 2014, Heat Treatment of Metals, Beijing, China, vol. 39, no. 7, pp.47-49.
4. L. Hu, J. Chen, B. Wang, Q.Y. Liu, Z.H. Li, Effects of inclusion on hydrogen induced cracking susceptibility of pipeline steels under electrochemical hydrogen-charging condition, 2015, Materials for Mechanical Engineering, vol. 39, no. 9, pp.25-31.

5. X.G. Zeng, K. Liu, H. Luo, C.S. Luo, J.H. Zhao J, Study on mechanical behavior of N80 pipeline steel after electrochemical Hydrogen Charging, 2013, Hot Working Technology, vol. 44, no. 6, pp.41-44.
6. Z.X. Wang, B.P. Qu, F. Xue, H. Yang, Experimental investigation of hydrogen embrittlement of 65Mn steel with small punch testing method, 2011, Nuclear Power Engineering, vol. 32, no. 4, pp.14-18.
7. F.S. Du, Y. Li, M. Wang, J. Li, J.K. Fan. Macro-meso cross-scale simulation of forging process, 2014, Chinese Journal of Computational Mechanics, vol. 31, no. 6, pp.799-810.
8. W.Y. Chu, J.X. Li, Y.J. Su, L.J. Qiao. Influence of inclusions on initiation of hydrogen blister in iron, 2007, Acta Metallurgica Sinica, vol. 243, no. 7, pp. 673-677.
9. C.F. Dong, Z.Y. Liu, X.G. Li, Y.F. Cheng. Effects of hydrogen-charging on the susceptibility of X100 pipeline steel to hydrogen-induced cracking, 2009, International journal of hydrogen energy, vol. 34, no24, pp.9879-9884.